

Dynamical loss functions shape landscape topography and improve learning in artificial neural networks

Eduardo Lavin¹ and Miguel Ruiz-García^{2,3,*}

¹*Department of Applied Mathematics, ETSII, Universidad Politécnica de Madrid, Madrid, Spain*

²*Departamento de Estructura de la Materia, Física Térmica y Electrónica, Universidad Complutense Madrid, 28040 Madrid, Spain*

³*GISC - Grupo Interdisciplinar de Sistemas Complejos, Universidad Complutense Madrid, 28040 Madrid, Spain*

(Dated: October 15, 2024)

Dynamical loss functions are derived from standard loss functions used in supervised classification tasks, but they are modified such that the contribution from each class periodically increases and decreases. These oscillations globally alter the loss landscape without affecting the global minima. In this paper, we demonstrate how to transform cross-entropy and mean squared error into dynamical loss functions. We begin by discussing the impact of increasing the size of the neural network or the learning rate on the learning process. Building on this intuition, we propose several versions of dynamical loss functions and show how they significantly improve validation accuracy for networks of varying sizes. Finally, we explore how the landscape of these dynamical loss functions evolves during training, highlighting the emergence of instabilities that may be linked to edge-of-instability minimization.

Most machine learning tasks reduce to the minimization of a loss function landscape in a high-dimensional parameter space [1–14]. Although this picture may look reminiscent of several problems in physics, e.g. the minimization of the energy of a system of soft-interacting particles or the process of tuning physical networks [15–25], the optimization (training) of deep neural networks (DNNs) challenges our physical intuition. Contrary to the smooth minimization of physical properties that we may have in mind, DNN minimization is characterized by instabilities. In particular, machine learning minimization typically occurs in regions of the landscape where only a few eigenvalues of the Hessian are clearly positive, whereas the rest of the eigenvalues remain close to zero or even take negative values [26–31]. Within the subspace spanned by these outliers of the Hessian, the loss function landscape typically displays a valley-like structure, and the model descends it towards regions of smaller values of the loss. During this minimization process, the model oscillates between the walls of the valley [32] and can become trapped if it reaches a region where the valley is too narrow for the minimization step to proceed. In such cases, if the model fails to find a wider valley, it can lead to *edge of stability* minimization [33–35].

The ubiquity of edge-of-stability minimization in deep learning [33], at odds with the intuition gained from most physical systems, presents an opportunity for new understanding and for the exploration of alternative optimization techniques. We think that dynamical loss func-

tions [36] can allow us to tackle both questions ¹. These loss functions – weighted by class with weights that oscillate during minimization – are reminiscent of other oscillating strategies in biological systems, materials science and physics that lead to better solutions [37–42]. We think that studying the interplay between edge-of-stability minimization and dynamical loss functions can pave the path for understanding how the topography of the loss function landscape shapes learning and how modifying this topography can improve the behavior of deep learning.

In supervised classification tasks, the loss function \mathcal{F} is defined such that its global minima ($\mathcal{F} = 0$) correspond to the correct classification of the *training* dataset. In the case of cross-entropy:

$$\mathcal{F}_{\text{CE}} = \sum_{j \leq P} -\log \left(\frac{e^{f_{y_j}(x_j, \mathbf{W})}}{\sum_i e^{f_i(x_j, \mathbf{W})}} \right), \quad (1)$$

where x_j is an element of the training set of size P , y_j is its label/class, and $f(x_j, \mathbf{W}) \in \mathbb{R}^C$ is the logit output of the neural network given trainable parameters \mathbf{W} (C is the number of classes). Learning in this type of problems boils down to the minimization of the loss function, and reaching the global minima strongly depends on the number of parameters present in the neural network (\mathbf{W})

¹ Code reproducing some of our main results can be found at <https://github.com/miguel-rg/dynamical-loss-functions>.

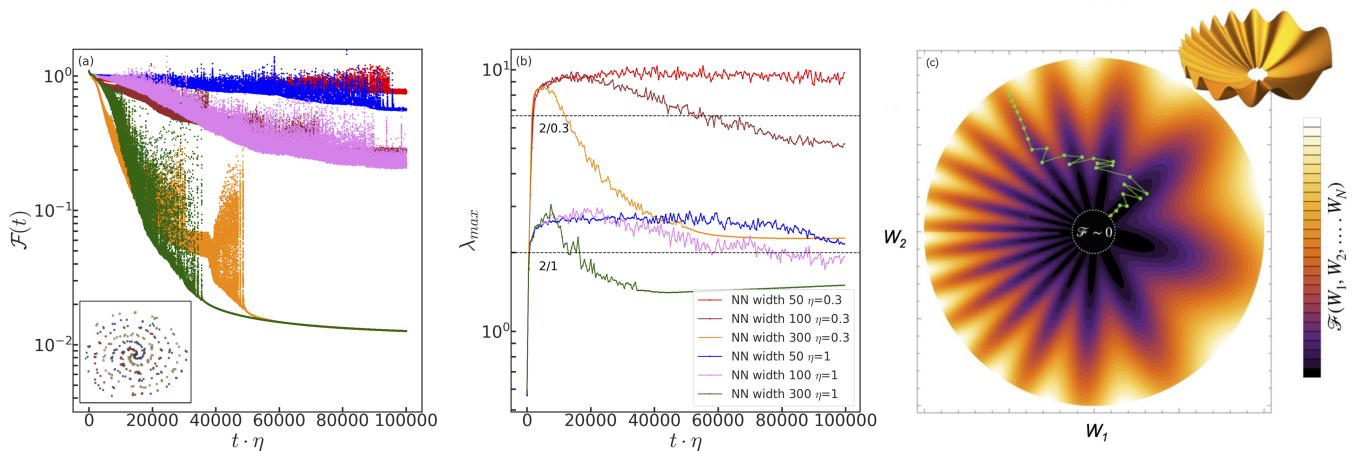


FIG. 1. Interplay between network size and learning rate in the minimization of cross-entropy loss function. For three different network sizes and two different learning rates (η) we average the instantaneous values of the loss function and curvature (largest eigenvalue of the Hessian, λ_{max}) during the minimization of 20 simulations. The training dataset is presented in the inset of panel (a)—2D points belonging to three classes that follow the three arms of a spiral. Panel (a) shows the mean value of the loss, whereas (b) shows the mean value of the largest eigenvalue of the Hessian. Spikes during training (edge-of-stability minimization) is most clear in panel (a). Panel (b) shows how smaller learning rates can reach narrower valleys, although this does not translate to better training. Even so, we see that for large network sizes the system tends to reach wider valleys for both learning rates. Panel (c) shows a toy representation of the loss function landscape that can qualitatively explain the behavior of panels (a) and (b). We represent a subspace of parameter space, that displays in its center a global minimum that occupies a finite region of parameter space. Valleys that lead to the global minimum need to increase their sharpness to fit into the boundary. Minimization in this landscape (green dots) can lead to instabilities due to the increase in curvature as the system approaches the minimum. During the instabilities the system can jump towards wider valleys and in some cases it can find one that is wide enough to smoothly descend into the minimum.

compared with the amount (or complexity) of the data. Classic bias-variance tradeoff suggests that too few parameters (\mathbf{W}) will not be enough to learn the data (underparametrized regime), whereas too many parameters will lead to overfitting, damaging generalization (overparametrized regime). However, neural networks have been shown to generalize best in the overparametrized regime [43–47]. This paper shows how dynamical loss functions reduce the critical number of parameters that leads to overparameterization, allowing the reduction of computational costs and potentially improving generalization.

First, we study how minimization develops for different network sizes and learning rates in a toy problem with standard (nondynamical) cross entropy. We use a fully connected neural network (NN) with one hidden layer of variable width. We compute the Hessian of the loss during minimization, where its largest eigenvalue indicates the *sharpness* [33, 48]. Fig. 1 displays three NN widths and two different learning rates. Panel (a) shows how learning improves as the network size increases—the system can find a basin that is wide enough to get to the global minimum. However, learning also improves when learning rate increases. Panel (b) shows how the local curvature evolves during training. For all the cases, minimization starts in regions with smooth curvature and the

system quickly moves to a region where the largest eigenvalue is slightly above $2/\eta$. This phenomenon is consistent with edge-of-stability (EoS) minimization. For the largest network, the system finds a way to scape EoS and enters a region of high curvature. Panel (c) provides a qualitative explanation of this phenomenon. This panel presents a cartoon representation of the loss function landscape that can explain the main phenomenology presented in panels (a) and (b). We hypothesize that typical loss function landscapes in NNs are characterized by global minima that occupy bounded regions of parameter space and are surrounded by valleys that descend towards them (this is consistent with recent work [49]). Due to the finite size of the $\mathcal{F} \sim 0$ regions, the valleys need to increase their sharpness to fit along the boundary of the global minima. As the system descends a valley (green dots) the curvature increases until the minimization becomes unstable. Then, the NN can jump sequentially from one valley to another, descending the loss landscape while maintaining approximately the same curvature. Increasing the NN width leads to a parameter space of higher dimension and wider valleys. When the dimension is high enough, the NN will explore several valleys (EoS phase) until it finds a valley that is wide enough to descend to the global minimum. Even more, larger learning rates explore larger portions of the landscape as they try to find a valley that is wide enough, which they

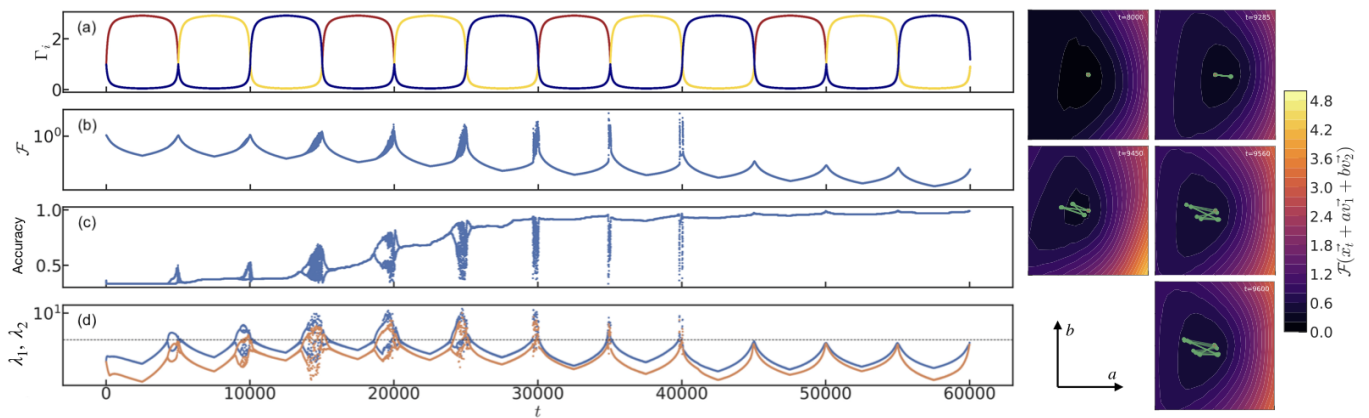


FIG. 2. Evolution of learning with a dynamical loss function. Panel (a) shows the evolution of the parameters Γ_i which control the change of the dynamical loss function $\mathcal{F}(t)$. Panel (b) displays the instantaneous value of the loss during training, whereas panels (c) and (d) show the training accuracy and the two largest eigenvalues of the Hessian (λ_1 and λ_2), respectively. Finally, the panels at the right display the evolution of the system as it approaches the last part of one of the oscillations, where instabilities emerge. We represent a subspace of parameter space spanned by the eigenvectors associated to the two largest eigenvalues of the Hessian, \vec{v}_1 and \vec{v}_2 , where a and b take values in $[-1, 1]$. The background color displays the value of \mathcal{F} around the point in parameter space where the system is at $t = 8000, 9285, 9450, 9560$ and 9600 (\vec{x}_t , a red cross in the plots). Green dots represent the position of the system at times $\{t, t+1, \dots, t+20\}$, and they are connected by semitransparent green arrows. We use a neural network with one hidden layer of width 100 and full batch gradient descent, where $T = 5000$ and $A = 70$ (see SM), chosen for ease of visualization.

descend more quickly. Counterintuitively, minimization instabilities can be harnessed to find better regions of the landscape [33, 36, 50].

We show now how dynamical loss functions can lead to sequential instabilities and a larger exploration of parameter space, improving generalization and allowing us to use smaller NNs. First we carry out a simple variation of cross-entropy, that we will denote dynamical cross entropy (DCE):

$$\mathcal{F}_{\text{DCE}} = \sum_{j \leq P} \Gamma_{y_j}(t) \left(-\log \left(\frac{e^{f_{y_j}(x_j, \mathbf{W})}}{\sum_i e^{f_i(x_j, \mathbf{W})}} \right) \right) \quad (2)$$

Where Γ_i is a different oscillating factor for *each class* i , and t is the number of minimization steps. Depending on the values of Γ_i , the topography of the loss function will change, but the loss function will still vanish at the same global minima, which are unaffected by the value of Γ_i . This transformation was motivated by recent work in which the topography of the loss function was changed to improve the tuning of physical flow networks [25]. We use Γ_i to emphasize one class relative to the others for a period T , and cycle through all the classes in turn so that the total duration of a cycle that passes through all classes is CT . Figure 2 (a) shows the oscillating factors Γ_i that we use in the case of DCE for the case of the dataset with three classes shown in Fig. 1, these oscillations are controlled by two parameters, their amplitude (A) and period (T). The specific expression for $\Gamma_i(t)$ are detailed in the Supplementary Materials. In the

case $A \gg 1$, the model can easily find a global minimum (the network would output the chosen class regardless of input) without making any uphill moves, and therefore the landscape is convex. However, in the next period the network will have to learn a different class, suggesting that the transition between periods will mark the points at which the topography of the landscape becomes more complex—note that right at the transition all Γ_i are 1 and we recover the standard loss function.

The behavior of the system as it locally minimizes the dynamical loss function landscape is summarized in Fig. 2. In the first half of each period T the instantaneous value of \mathcal{F}_{DCE} and the largest eigenvalues of the Hessian (curvature) decrease, whereas the accuracy stays flat. The system is descending a valley that shifts downwards and also widens. In the second half of each oscillation, the valley narrows and rises (\mathcal{F} increases even though the system is undergoing gradient descent; see panel (b)). Additionally, something remarkable happens when the largest eigenvalue of the Hessian crosses the value $2/\eta$, marked by the horizontal dashed line in panel (d): a bifurcation emerges, clearly visible in panel (c). There are additional bifurcations each time another eigenvalue reaches $2/\eta$, forming a period-doubling cascade. These bifurcations correspond to the system bouncing between the walls of the valley, this is clearly depicted by the panels that show a section of parameter space along the eigenvectors associated to the two largest eigenvalues of the Hessian. As time approaches $t = 10000$ we see how the system starts bouncing between two walls,

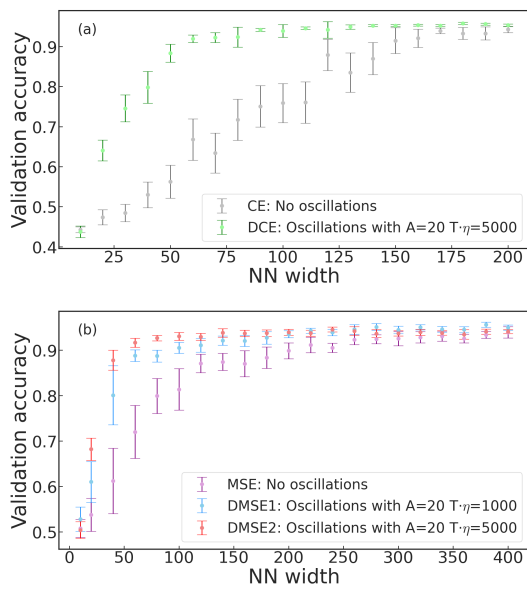


FIG. 3. Dynamical loss functions can train smaller networks. We use again a fully connected DNN and the Swiss Roll dataset as in Fig. 1 (b). The validation dataset in both cases is similar to the training dataset but generated with a different seed leading to a different distribution of the points along the spiral. In panel (a) we compare CE and DCE with $\eta = 1$, and we average 50 simulations for each NN size. In panel (b) we compare MSE with the two versions of DMSE with $\eta = 0.075$, and average 10 simulations for each NN size. In both panels we change $A = 1$ (static loss) for the last oscillation where we measure the accuracy, showing that dynamical loss functions take the system to a different region of parameter space (compared to their static versions) where validation accuracy improves. The errorbars display the error of the mean.

four, etc. . . Remarkably, these instabilities do not destroy learning but seem to enhance it—see how accuracy keeps increasing during the bifurcation cascades.

We also propose two different dynamical loss functions based on mean square error (MSE):

$$\mathcal{F}_{\text{DMSE}_1} = \frac{1}{N} \sum_{j \leq P} \Gamma_i(t) \sum_{i \leq C} (f_i(\mathbf{x}_j, \mathbf{W}) - y_{j,i})^2, \quad (3)$$

$$\mathcal{F}_{\text{DMSE}_2} = \frac{1}{N} \sum_{j \leq P} \sum_{i \leq C} (f_i(\mathbf{x}_j, \mathbf{W}) - \Gamma_i(t)y_{j,i})^2, \quad (4)$$

see the Supplementary Materials for a detailed explanation of their behavior. Despite their differences, we observe that DMSE1 and DMSE2 both display bifurcations reminiscent of Fig. 2 and can improve learning and generalization. Fig. 3 shows how dynamical loss functions improve validation accuracy over their corresponding standard static loss (CE or MSE). This difference is greatest for small network sizes—dynamical loss functions shift

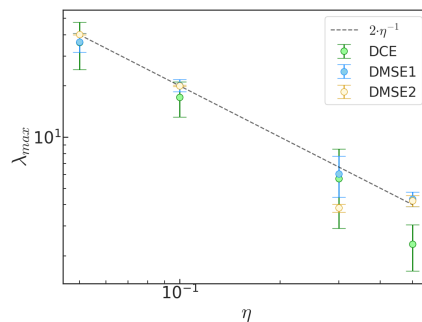


FIG. 4. We represent the value of λ_{\max} at which instabilities emerge (see Fig. 2 (d)) vs η . To show the robustness of the result, we simulate different conditions: $A = [25, 50, 75]$, $T = [5,000, 10,000]$ for a total time $T_{\text{total}} = 100,000/\eta$, with $NN_{\text{width}} = 100$. We represent the mean value of 30 simulations per condition. The dash line is the prediction from edge-of-stability minimization. The error bars display the error of the mean.

the under to over-parameterized transition—but validation accuracy is also higher for the dynamical loss function at large NN sizes. To explore the effect on system size in Fig. 3 we have selected a specific amplitude and period for the oscillations. There is a region in hyperparameter space (amplitude and period) that improves the results of standard loss functions (see supplementary material), although the results can also deteriorate when the amplitude and period become too large, and catastrophic forgetting can occur [51, 52]. To further explore the similarities between DCE, DMSE1 and DMSE2, and their connection with edge-of-stability minimization, we present in Fig. 4 the relationship between the mean value of the Hessian largest eigenvalue at which the first instability occurs for different learning rates. We see how the relationship between curvature and learning rate displays the same scaling for DCE, DMSE1 and DMSE2, compatible with $2/\eta$, the theoretical prediction from ‘*edge of stability*’ minimization [33].

This letter explores the behavior of dynamical loss functions, a new approach to learning in deep neural networks that has deep connections to fundamental problems in physics [25, 33, 37–42, 49]. We have shown how this approach can improve the behavior of NNs, reducing the critical size at which overparametrization begins. Dynamical loss functions open a new plethora of possibilities to explore how changing the topography of the loss function landscape during minimization can control (and improve) learning in deep neural networks. We think that dynamical loss functions can become a workbench for the physics community to understand the connections between landscape topography and learning in artificial neural networks.

Acknowledgements

We acknowledge support from the Ramón y Cajal program (RYC2021-032055-I), the Human Frontiers Science Program (RGE33/2024), the Spanish Research Agency (PID2023-147067NB-I00), and from the CONEX-Plus program funded by Universidad Carlos III de Madrid and the European Union’s Horizon 2020 research and innovation program under the Marie Skłodowska-Curie grant agreement No. 801538.

* miguel.ruiz.garcia@ucm.es

- [1] L. Rosasco, E. D. Vito, A. Caponnetto, M. Piana, and A. Verri, Are loss functions all the same?, *Neural Computation* **16**, 1063 (2004).
- [2] A. Choromanska, M. Henaff, M. Mathieu, G. B. Arous, and Y. LeCun, The loss surfaces of multilayer networks, in *Artificial intelligence and statistics* (PMLR, 2015) pp. 192–204.
- [3] H. Li, Z. Xu, G. Taylor, C. Studer, and T. Goldstein, Visualizing the loss landscape of neural nets, *Advances in neural information processing systems* **31** (2018).
- [4] D. Soudry and Y. Carmon, No bad local minima: Data independent training error guarantees for multilayer neural networks, arXiv preprint arXiv:1605.08361 (2016).
- [5] Y. Cooper, The loss landscape of overparameterized neural networks, arXiv preprint arXiv:1804.10200 (2018).
- [6] P. C. Verpoort, D. J. Wales, *et al.*, Archetypal landscapes for deep neural networks, *Proceedings of the National Academy of Sciences* **117**, 21857 (2020).
- [7] K. Janocha and W. M. Czarnecki, On loss functions for deep neural networks in classification, arXiv preprint arXiv:1702.05659 (2017).
- [8] S. Kornblith, H. Lee, T. Chen, and M. Norouzi, What’s in a loss function for image classification?, arXiv preprint arXiv:2010.16402 (2020).
- [9] A. J. Ballard, R. Das, S. Martiniani, D. Mehta, L. Sagun, J. D. Stevenson, and D. J. Wales, Energy landscapes for machine learning, *Physical Chemistry Chemical Physics* **19**, 12585 (2017).
- [10] S. S. Mannelli, G. Biroli, C. Cammarota, F. Krzakala, and L. Zdeborová, Who is afraid of big bad minima? analysis of gradient-flow in a spiked matrix-tensor model, arXiv preprint arXiv:1907.08226 (2019).
- [11] G. B. Arous, S. Mei, A. Montanari, and M. Nica, The landscape of the spiked tensor model, *Communications on Pure and Applied Mathematics* **72**, 2282 (2019).
- [12] M. Goldblum, J. Geiping, A. Schwarzschild, M. Moeller, and T. Goldstein, Truth or backpropaganda? an empirical investigation of deep learning theory, arXiv preprint arXiv:1910.00359 (2019).
- [13] M. P. Niroomand, L. Dicks, E. Pyzer-Knapp, and D. J. Wales, Explainable gaussian processes: a loss landscape perspective, *Machine Learning: Science and Technology* (2024).
- [14] M. P. Niroomand, L. Dicks, E. O. Pyzer-Knapp, and D. J. Wales, Insights into machine learning models from chemical physics: an energy landscapes approach (el for ml), *Digital Discovery* **3**, 637 (2024).
- [15] S. Franz and G. Parisi, The simplest model of jamming, *Journal of Physics A: Mathematical and Theoretical* **49**, 145001 (2016).
- [16] M. Geiger, S. Spigler, S. d’Ascoli, L. Sagun, M. Baity-Jesi, G. Biroli, and M. Wyart, Jamming transition as a paradigm to understand the loss landscape of deep neural networks, *Physical Review E* **100**, 012115 (2019).
- [17] S. Franz, S. Hwang, and P. Urbani, Jamming in multilayer supervised learning models, *Physical review letters* **123**, 160602 (2019).
- [18] S. Franz, A. Sclocchi, and P. Urbani, Critical jammed phase of the linear perceptron, *Physical review letters* **123**, 115702 (2019).
- [19] M. Geiger, A. Jacot, S. Spigler, F. Gabriel, L. Sagun, S. d’Ascoli, G. Biroli, C. Hongler, and M. Wyart, Scaling description of generalization with number of parameters in deep learning, *Journal of Statistical Mechanics: Theory and Experiment* **2020**, 023401 (2020).
- [20] M. Geiger, L. Petrini, and M. Wyart, Perspective: A phase diagram for deep learning unifying jamming, feature learning and lazy training, arXiv preprint arXiv:2012.15110 (2020).
- [21] M. Ruiz-Garcia, L. Bonilla, and A. Prados, Bifurcation analysis and phase diagram of a spin-string model with buckled states, *Physical Review E* **96**, 062147 (2017).
- [22] J. W. Rocks, N. Pashine, I. Bischofberger, C. P. Goodrich, A. J. Liu, and S. R. Nagel, Designing allosteric-inspired response in mechanical networks, *Proceedings of the National Academy of Sciences* **114**, 2520 (2017).
- [23] L. Yan, R. Ravasio, C. Brito, and M. Wyart, Architecture and coevolution of allosteric materials, *Proceedings of the National Academy of Sciences* **114**, 2526 (2017).
- [24] J. W. Rocks, H. Ronellenfitsch, A. J. Liu, S. R. Nagel, and E. Katifori, Limits of multifunctionality in tunable networks, *Proceedings of the National Academy of Sciences* **116**, 2506 (2019).
- [25] M. Ruiz-García, A. J. Liu, and E. Katifori, Tuning and jamming reduced to their minima, *Physical Review E* **100**, 052608 (2019).
- [26] L. Sagun, U. Evci, V. U. Guney, Y. Dauphin, and L. Bottou, Empirical analysis of the hessian of over-parametrized neural networks, arXiv preprint arXiv:1706.04454 (2017).
- [27] L. Sagun, L. Bottou, and Y. LeCun, Eigenvalues of the hessian in deep learning: Singularity and beyond, arXiv preprint arXiv:1611.07476 (2016).
- [28] A. R. Sankar, Y. Khasbage, R. Vigneswaran, and V. N. Balasubramanian, A deeper look at the hessian eigenspectrum of deep neural networks and its applications to regularization, in *Proceedings of the AAAI Conference on Artificial Intelligence*, Vol. 35 (2021) pp. 9481–9488.
- [29] Z. Yao, A. Gholami, K. Keutzer, and M. W. Mahoney, Pyhessian: Neural networks through the lens of the hessian, in *2020 IEEE international conference on big data (Big data)* (IEEE, 2020) pp. 581–590.
- [30] K. Ahn, J. Zhang, and S. Sra, Understanding the unstable convergence of gradient descent, in *International Conference on Machine Learning* (PMLR, 2022) pp. 247–257.
- [31] S. Kaur, J. Cohen, and Z. C. Lipton, On the maximum hessian eigenvalue and generalization, in *Proceedings on* (PMLR, 2023) pp. 51–65.

- [32] C. Xing, D. Arpit, C. Tsirigotis, and Y. Bengio, A walk with sgd, arXiv preprint arXiv:1802.08770 (2018).
- [33] J. M. Cohen, S. Kaur, Y. Li, J. Z. Kolter, and A. Talwalkar, Gradient descent on neural networks typically occurs at the edge of stability (2022), arXiv:2103.00065 [cs.LG].
- [34] X. Zhu, Z. Wang, X. Wang, M. Zhou, and R. Ge, Understanding edge-of-stability training dynamics with a minimalist example, arXiv preprint arXiv:2210.03294 (2022).
- [35] S. Arora, Z. Li, and A. Panigrahi, Understanding gradient descent on the edge of stability in deep learning, in *International Conference on Machine Learning* (PMLR, 2022) pp. 948–1024.
- [36] M. Ruiz-Garcia, G. Zhang, S. S. Schoenholz, and A. J. Liu, Tilting the playing field: Dynamical loss functions for machine learning, in *International Conference on Machine Learning* (PMLR, 2021) pp. 9157–9167.
- [37] A. Murugan and H. M. Jaeger, Bioinspired nonequilibrium search for novel materials, *MRS Bulletin* **44**, 96 (2019).
- [38] A. Murugan, K. Husain, M. J. Rust, C. Hepler, J. Bass, J. M. Pietsch, P. S. Swain, S. G. Jena, J. E. Toettcher, A. K. Chakraborty, *et al.*, Roadmap on biology in time varying environments, *Physical biology* **18**, 041502 (2021).
- [39] V. Mustonen and M. Lässig, From fitness landscapes to seascapes: non-equilibrium dynamics of selection and adaptation, *Trends in genetics* **25**, 111 (2009).
- [40] L. Di Bari, M. Bisardi, S. Cotogno, M. Weigt, and F. Zamponi, Emergent time scales of epistasis in protein evolution, *bioRxiv*, 2024 (2024).
- [41] J. Cairns, F. Borse, T. Mononen, T. Hiltunen, and V. Mustonen, Strong selective environments determine evolutionary outcome in time-dependent fitness seascapes, *Evolution Letters* **6**, 266 (2022).
- [42] M. J. Falk, J. Wu, A. Matthews, V. Sachdeva, N. Pashine, M. L. Gardel, S. R. Nagel, and A. Murugan, Learning to learn by using nonequilibrium training protocols for adaptable materials, *Proceedings of the National Academy of Sciences* **120**, e2219558120 (2023).
- [43] M. Belkin, D. Hsu, S. Ma, and S. Mandal, Reconciling modern machine-learning practice and the classical bias–variance trade-off, *Proceedings of the National Academy of Sciences* **116**, 15849 (2019).
- [44] C. Zhang, S. Bengio, M. Hardt, B. Recht, and O. Vinyals, Understanding deep learning (still) requires rethinking generalization, *Communications of the ACM* **64**, 107 (2021).
- [45] P. Nakkiran, G. Kaplun, Y. Bansal, T. Yang, B. Barak, and I. Sutskever, Deep double descent: Where bigger models and more data hurt, *Journal of Statistical Mechanics: Theory and Experiment* **2021**, 124003 (2021).
- [46] S. d’Ascoli, M. Refinetti, G. Biroli, and F. Krzakala, Double trouble in double descent: Bias and variance (s) in the lazy regime, in *International Conference on Machine Learning* (PMLR, 2020) pp. 2280–2290.
- [47] J. W. Rocks and P. Mehta, Memorizing without overfitting: Bias, variance, and interpolation in overparameterized models, *Physical review research* **4**, 013201 (2022).
- [48] G. Gur-Ari, D. A. Roberts, and E. Dyer, Gradient descent happens in a tiny subspace, arXiv preprint arXiv:1812.04754 (2018).
- [49] B. L. Annesi, C. Lauditi, C. Lucibello, E. M. Malatesta, G. Perugini, F. Pittorino, and L. Saglietti, Star-shaped space of solutions of the spherical negative perceptron, *Physical Review Letters* **131**, 227301 (2023).
- [50] A. Lewkowycz, Y. Bahri, E. Dyer, J. Sohl-Dickstein, and G. Gur-Ari, The large learning rate phase of deep learning: the catapult mechanism, arXiv preprint arXiv:2003.02218 (2020).
- [51] M. McCloskey and N. J. Cohen, Catastrophic interference in connectionist networks: The sequential learning problem, in *Psychology of learning and motivation*, Vol. 24 (Elsevier, 1989) pp. 109–165.
- [52] M. Ruiz-Garcia, Model architecture can transform catastrophic forgetting into positive transfer, *Scientific Reports* **12**, 10736 (2022).